POTENTIAL CLINICAL RELEVANCE

Nanomedicine: Nanotechnology, Biology, and Medicine
9 (2013) 1124–1134

Feature Article

nanomedjournal.com

Nanoparticles for urothelium penetration and delivery of the histone deacetylase inhibitor belinostat for treatment of bladder cancer

Darryl T. Martin, PhD[a,1], Christopher J. Hoimes, DO[b,c,1], Hristos Z. Kaimakliotis, MD[a], Christopher J. Cheng, PhD[b], Ke Zhang, PhD[d], Jingchun Liu, MD, PhD[a], Marcia A. Wheeler, MS[a], W. Kevin Kelly, DO[g], Greg N. Tew, PhD[d,e,f], W. Mark Saltzman, PhD[b], Robert M. Weiss, MD[a,*]

[a]*Department of Urology, Yale University, New Haven, CT*
[b]*Department of Biomedical Engineering, Yale University, New Haven, CT*
[c]*Department of Medical Oncology, Yale University, New Haven, CT*
[d]*Departments of Polymer Science & Engineering, University of Massachusetts, Amherst, MA*
[e]*Veterinary & Animal Sciences, University of Massachusetts, Amherst, MA*
[f]*Molecular & Cellular Biology, University of Massachusetts, Amherst, MA*
[g]*Department of Medical Oncology and Urology, Thomas Jefferson University, Philadelphia, PA*

Received 4 April 2013; accepted 20 May 2013

Abstract

Nearly 40% of patients with non-invasive bladder cancer will progress to invasive disease despite locally-directed therapy. Overcoming the bladder permeability barrier (BPB) is a challenge for intravesical drug delivery. Using the fluorophore coumarin (C6), we synthesized C6-loaded poly(lactide-co-glycolide) (PLGA) nanoparticles (NPs), which were surface modified with a novel cell penetrating polymer, poly(guanidinium oxanorbornene) (PGON). Addition of PGON to the NP surface improved tissue penetration by 10-fold in intravesically-treated mouse bladder and *ex vivo* human ureter. In addition, NP-C6-PGON significantly enhanced intracellular uptake of NPs compared to NPs without PGON. To examine biological activity, we synthesized NPs that were loaded with the histone deacetylase (HDAC) inhibitor belinostat (NP-Bel-PGON). NP-Bel-PGON exhibited a significantly lower IC50 in cultured bladder cancer cells, and sustained hyperacetylation, when compared to unencapsulated belinostat. Xenograft tumors treated with NP-Bel-PGON showed a 70% reduction in volume, and a 2.5-fold higher intratumoral acetyl-H4, when compared to tumors treated with unloaded NP-PGON.

From the Clinical Editor: These authors demonstrate that PLGA nanoparticles with PGON surface functionalization result in greatly enhanced cell penetrating capabilities, and present convincing data from a mouse model of bladder cancer for increased chemotherapy efficacy.

Key words: PLGA; Nanoparticle; Poly(guanidinium oxanorbornene); Bladder cancer; Belinostat

Seventy-five percent of bladder cancer patients in the United States have non-muscle invasive disease at diagnosis,[1] and transurethral resection of the tumor nodule is the primary treatment. Most patients also are considered for additional intravesical therapy with Bacillus Calmette-Guérin (BCG), which has been shown to be effective at reducing recurrence. However, the response to BCG is unpredictable with nearly 40% of patients developing invasive disease progression despite BCG treatment.[2] Thus, improving local therapeutic modalities is crucial for improving the treatment of non-muscle invasive disease. As the bladder wall is poorly vascularized, systemic treatments do not reach sufficient levels, efforts are aimed at better penetration of the bladder permeability barrier (BPB). The urothelium is stratified and comprised of basal cells, intermediate cells, and the luminal surface BPB, which is formed by umbrella cells joined by tight junctions, and covered by uroplakin

Role of the funding source: This publication was supported in part by the National Institutes of Health (NIH) grants 5RC1DK087015, UL1 RR0204139, and R01 EB000487; the Department of Defense (DOD) training award number W81XWH-10-1-0295; and the National Science Foundation (CHE-0910963).

Competing interests: There are no competing interests to report.

*Corresponding author: Department of Urology, Yale University, New Haven, CT.

E-mail address: robert.weiss@yale.edu (R.M. Weiss).

[1] These authors contributed equally to this work.

1549-9634/$ – see front matter © 2013 Elsevier Inc. All rights reserved.
http://dx.doi.org/10.1016/j.nano.2013.05.017

plaques.[3] Advantages of intravesical instillation of drugs include reduced systemic side effects and increased drug dose in the bladder tissue.[3] However, challenges include low BPB penetration and short drug exposure due to dilution during filling or elimination during voiding.

Improved outcomes were demonstrated in patients treated with a device that used positive charged ions to enhance BPB penetration of mitomycin C (MMC) compared to MMC alone.[4–6] Despite these encouraging results, implementing electromotive drug therapy into standard practice has been slow and generally not available outside of European academic centers.[7] To eliminate the need for a complex delivery device and to improve drug delivery through the urothelium, we have designed poly(guanidinium oxanorbornene) (PGON) surface functionalized poly(lactide-co-glycolide) (PLGA) nanoparticles (NPs) that can efficiently attach to the bladder urothelium and internalize into urothelial and bladder cancer cells for payload delivery.

Inhibition of histone deacetylases (HDACs) provides a strategy to halt invasion and metastasis of non-muscle invasive urothelial carcinoma. Histone acetylation is regulated by two families of enzymes, histone acetyl transferases and HDACs, which catalyze the addition or the removal of acetyl groups to lysine residues of nucleosomal histones, respectively. Approximately 5% of the total genome is regulated by HDACs, which affect genes involved in cellular proliferation, invasion, and metastasis,[8–10] and can be targeted with HDAC inhibitors.[11]

Belinostat (NSC726630, PXD101) is an hydroxamic acid HDAC inhibitor, which binds to the zinc finger on HDAC, resulting in the inhibition of HDACs, including the HDAC6 isoform, which is thought to be instrumental in migration and invasion of neoplasia.[12] Belinostat has been shown to induce growth inhibition and cell cycle arrest in *in vitro*, and has efficacy against non-muscle invasive urothelial cancers in transgenic and xenograft models.[13,14] Additionally, belinostat and other hydroxamic acid HDAC inhibitors have been shown to decrease invasion of bladder cancer in *in vitro* assays.[15,16] These features have led to a randomized clinical trial of HDAC inhibition for chemoprevention of urothelial cancers.[17] In Phase I and II trials of advanced tumors, belinostat was well tolerated, with a half-life of approximately 1 h.[18] Intravesical treatment of bladder cancer with belinostat has not been attempted in clinical trials, in part due to its limited water solubility and the need for a suitable carrier.

PLGA is a biocompatible, degradable polymer approved by the FDA that has been used to encapsulate and deliver drugs, siRNAs, DNAs, peptides, and proteins.[19,20] PLGA-NPs are particularly useful for stabilizing agents *in vivo*,[21] carrying agents across cellular or tissue barriers,[22] targeting specific cell populations,[23] and enhancing the delivery and biological activity of drugs and genetic agents.[24,25] To increase transurothelial penetration, migration, and tumor cell uptake of NPs, PLGA-NPs were coated with PGON or chitosan using pegylated (PEG) phospholipids[25] and acylated avidin,[26] respectively. PGON is a polymer based synthetic mimic of cell penetrating peptides[27] and lacks mammalian toxicity.[28] We previously showed that conjugating biotinylated chitosan to PLGA increases the uptake of PLGA-NPs into bladder cancer cells, as well as into normal bladder and ureteral tissues.[29]

Herein, we have characterized belinostat-loaded nanoparticles functionalized with chitosan and PGON. PGON-functionalized NPs were able to penetrate the urothelium of mouse bladder and human ureter, and a loaded higher belinostat (NP-Bel-PGON) payload than those that were chitosan-functionalized. NP-Bel-PGON induced prolonged HDAC inhibition *in vitro* and *in vivo* and suppressed bladder tumor growth in a xenograft.

Methods

Nanoparticle materials

Poly(D,L-lactide-co-glycolide) with terminal ester groups (PLGA, 50:50 monomer ratio and 0.55–0.75 dL/g inherent viscosity) was purchased from Durect Corporation. 1,2-distearoyl-sn-glycero-3-phosphoethanolamine-*N*-[carboxy(polyethylene glycol)-2000] (DSPE-PEG) and DSPE-PEG-amine, were purchased from Avanti Polar Lipids. Biotinylated chitosan (2.5 kDa) was purchased from CarboMer, and size resolved by membrane filtration.

Synthesis of DSPE-PEG-PGON

PGON-modified with an NHS ester and t-BOC protecting groups was synthesized as described with a nine guanidinium chain length.[28] PGON-NHS was dissolved in dimethylformamide and incubated overnight with DSPE-PEG-amine in borate buffer at room temperature. A 1:1 mixture of triethylamine and dichloromethane (DCM) was used to remove t-BOC. The reaction mixture was purified using a rotary evaporator and dialysis in PBS at pH 7.4.

Preparation of avidin-palmitic acid conjugates

PLGA-NPs were coated with palmitate-avidin and then conjugated to biotinylated chitosan using methods previously described.[26]

Nanoparticle fabrication

Ligand coated and unmodified PLGA-NPs containing belinostat were prepared using a modified oil-in-water single emulsion technique. Briefly, belinostat was solubilized with PLGA in1:3 methanol and DCM overnight, and the ligands (i.e. DSPE-PEG-PGON or palmitate-avidin) were added to 5% (w/v) poly(vinyl alcohol) (PVA) in water at 37 °C 30 min prior to use. The organic phase was added dropwise to the aqueous phase under vigorous vortexing. This mixture was then sonicated using a TMX 400 probe sonicator and immediately poured into 0.3% (w/v) PVA in water. The NPs were allowed to harden under continuous stirring for 12 h to allow full evaporation of the organic phase. NPs were then collected by centrifugation, washed three times with deionized water, lyophilized, and stored at −20°C. Morphology of gold sputter-coated particles was analyzed using an XL-30 scanning electron microscope (FEI). ImageJ software analysis was used to determine particle diameter. C6-loaded NPs were prepared similarly using C6 0.3% (w/w) and DCM solvent evaporation for 3 h. Nile-Red (NR)-loaded NPs were prepared using NR 0.2% (w/w) and ethyl acetate solvent evaporation for at least 6 h. NP encapsulant

loading was determined with DMSO dissolution or ethanol extraction and spectrofluorescence read against a respective standard curve.

Three NP treatment designs were used: 1) belinostat-loaded PLGA-NP functionalized with avidin (NP-Bel), 2) belinostat-loaded PLGA-NP functionalized with avidin and biotinylated chitosan (NP-Bel-Chit), 3) belinostat-loaded PLGA-NP functionalized with PEG phospholipids and PGON (NP-Bel-PGON). Also, empty-NP (lacking belinostat) served as a negative control (NP-Bk-PGON).

Cytotoxicity of bladder cancer cells

Three bladder cancer cell lines (T-24, UM-UC-3, and RT-4) were acquired from the American Type Culture Collection. T-24 and RT-4 cells were maintained in McCoy's medium, whereas UM-UC-3 cells were maintained in Eagles Minimum Essential medium. All cells were supplemented with 10% fetal bovine serum, 1% penicillin-streptomycin, and 1% glutamine. Bladder cancer cells were seeded at 5×10^3 cells/well in a 96-well plate. T-24 cells are derived from an invasive high-grade bladder tumor with metastatic potential, UM-UC-3 cells have high metastatic potential and commonly used in xenograft models whereas RT-4 cells are more differentiated cells that have a papillary non-invasive phenotype. Cells were treated for 72 h with increasing concentrations of unencapsulated belinostat, NP-Bel, NP-Bel-Chit, and/or NP-Bel-PGON. NP-Bk-PGON served as a control, and the amount added varied in relation to the concentration of belinostat. Viability was measured after removing the NPs by washing the plates with PBS buffer. Cell viability also was measured in the presence of increasing mass of NPs, regardless of the amount of belinostat that was encapsulated. Cell viability was measured using WST-1 Reagent (Clontech) and IC_{50}s were calculated after curve fitting of % inhibition of control value versus log concentration using Origin Lab Data Analysis Software.

NP uptake in ex vivo human ureter

The use of human tissue was approved by the Human Investigation Committee (#0710003157) at Yale University. The uptake of functionalized-NPs was measured in an *ex vivo* binding assay using benign human ureter within 4 h of collection. After washing the tissue in sterile DMEM with antibiotics, the tissue was placed in an autoclaved 96-well dot blot chamber (Biorad) with the luminal urothelium facing upward. Non-functionalized and functionalized NPs (200 μg NP/well) loaded with C6 were suspended in artificial urine and added to individual wells. Artificial urine was used as a control. The dot-blot chamber was then incubated at 37°C for up to 2 h. After incubation, wells were washed four times to remove non-adherent NPs, the tissue was cored, weighed, and extracted for fluorescence.

Mouse intravesical instillation

Female mice were sedated with ketamine (100 mg/kg) and xylazine (10 mg/kg) and then catheterized with a lubricated catheter from a 24G angiocath needle (BD). Bladders were emptied by manual compression and irrigated with sterile PBS, followed by instillation of 100 μl of NR encapsulated NPs including unmodified-NP (plain) and modified-NPs (PEG and PGON) at 1 mg/ml. An ultra-small clamp was placed on the external urethra for 2 h to prevent bladder emptying, after which the mouse bladder was washed extensively with PBS to remove non-adherent particles before the mouse was sacrificed and bladder removed. The bladders were then weighed and frozen for tissue extraction or embedded with OCT for fluorescence microscopy.

Table 1
Loading of belinostat.

NP formulation	Diameter (nm ± SD)	Loading (μg Bel/mg NP)
NP-Bel	144 ± 40	39 ± 0.63
NP-Bel-Chit	153 ± 25	19 ± 0.66
NP-Bel-PGON	151 ± 32	129 ± 3.1

Fluorescence extraction from human and mouse tissue

Distilled water (750 μl) was added to frozen tissue cores or mouse bladders and homogenized on ice using a polytron (Brinkmann Instruments). The homogenate was vortexed for one hr at room temperature using the highest speed and then centrifuged (16,000×*g*, 10 min). DMSO was added to the precipitate and was again vortexed and centrifuged. The fluorescence in the samples (100 μl aliquots) was measured using a spectrofluorimeter at 460 nm excitation, 540 nm emission. Fluorescence in the DMSO supernatant was divided by either total fluorescence to determine % fluorescence, or by mouse bladder or human tissue weight.

Fluorescence-activated cell sorting (FACS)

Bladder cancer cells were incubated with 1 mg/ml NP-C6 for 2 h in a 37 °C humidified chamber containing the appropriate medium. The cells were rinsed with cold medium to inhibit endocytosis before trypsinization. Subsequently, cells were either treated with 0.3% trypan blue for 2 min or untreated before being washed and fixed for FACS analysis.[31,32]

Fluorescence microscopy

For NP internalization studies, bladder cancer cells were grown on coverslips for 48 h until reaching 80–90% confluence. Cells were incubated with NP-C6s at 1 mg/ml for 2 h at 37 °C in a CO_2 incubator before the cells were rinsed with cold medium. Then the cells were treated with 0.3% trypan blue for 2 min or untreated before being washed with PBS and fixed in methanol-free 3.7% formaldehyde. Cells were then incubated with 0.1% Triton X-100 before being stained with Texas Red X-phalloidin (Invitrogen), to visualize actin. Coverslips with cells and cross-sections of mouse bladder were mounted on slides with Vectashield containing DAPI (Vector Laboratories) to visualize nuclei.

Xenograft Model

Eight-week-old female Foxn1 nu/nu mice were subcutaneously injected in the left flank with 10^7 UM-UC-3 bladder cancer cells that stably expressed red fluorescent protein (UM-UC-3R). Tumor volume was estimated using the formula (tumor length x tumor width^2) × π/6. One week after injection, when tumor

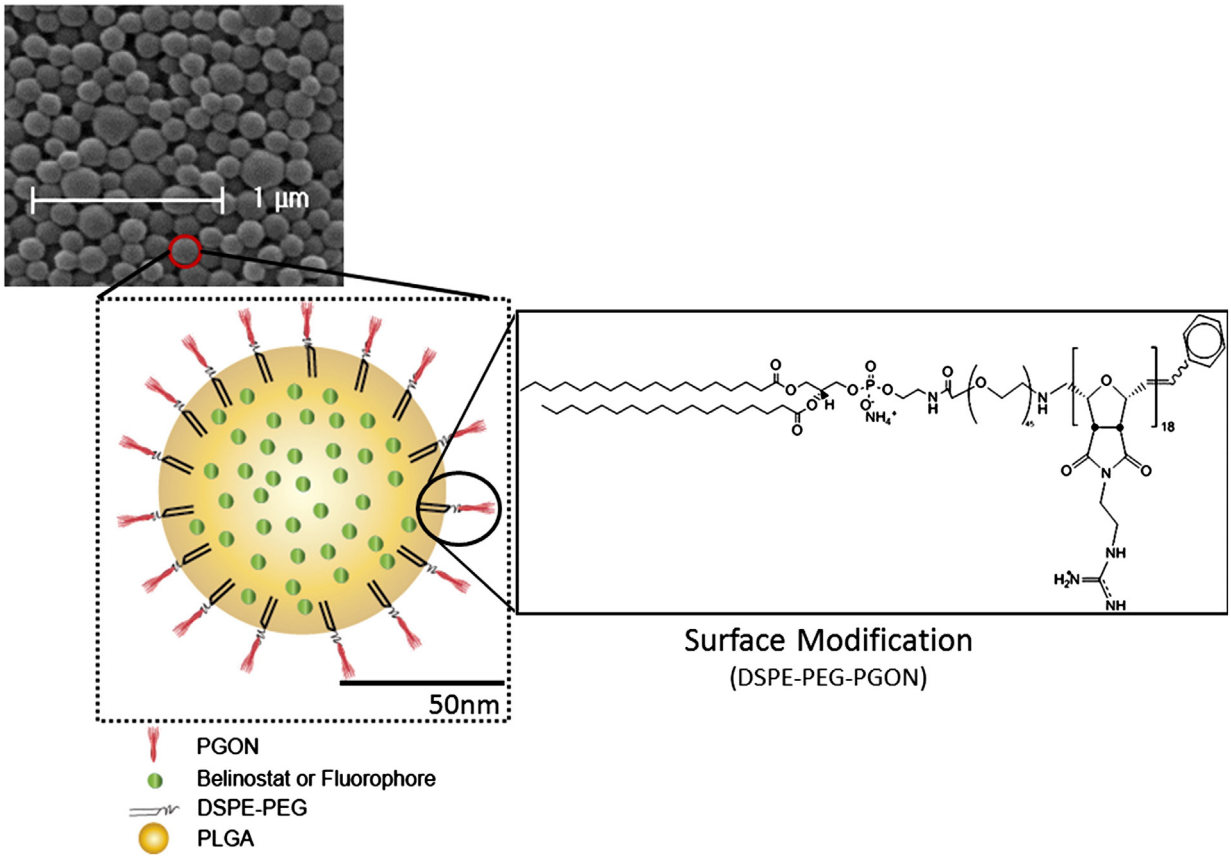

Figure 1. PGON-functionalized PLGA-NPs. Scanning electron micrograph of NP-PGON including a schematic diagram of the functionalized-NP containing fluorophore or belinostat.

volume was 243 ± 12 mm^3, mice were randomly divided into three groups: control (untreated) (n = 8); NP-Bk-PGON (n = 12); and NP-Bel-PGON (n = 10). Mice were intratumorally injected with 100 µl of the following: 10 mg/ml of NP-Bk-PGON or NP-Bel-PGON (5 mg belinostat/kg) diluted in PBS. Mouse tumors were injected on day 0, 4, 7, 11, 14 and 18, with day 0 being one week after injection of the tumor cells. Mouse tumors also were treated with 5 mg non-encapsulated belinostat/kg. Tumor volumes were measured prior to injections. All animals completed the study and were sacrificed on day 21 (28 days after cell inoculation). All xenograft mouse tumors were weighted, snap-frozen, and stored at −80°C. All animal studies were approved by the Institutional Animal Care and Use Committee of Yale University.

Western blot

Protein lysates were prepared from snap-frozen mouse tumors and human bladder cancer cells. Cells were lysed in RIPA buffer (Cell Signaling Technology) containing protease and phosphatase inhibitors that was supplemented with an EDTA-free protease inhibitor cocktail (Roche Applied Science), 1 mM NaF, 1 mM PMSF, and 2 µg/ml of Aprotinin. Mouse tumors were minced using a polytron homogenizer in RIPA buffer containing aforementioned inhibitors and protein lysates were quantified. Western blotting was based on modified protocols.[30,31] In brief, protein was analyzed by SDS-PAGE, transferred to PVDF membrane, blocked in 3% non-fat dry milk-PBS for 1 h at RT, and incubated with an acetyl-histone H4 rabbit polyclonal antibody (Millipore). Proteins were visualized with an anti-rabbit secondary conjugated to HRP, and detected using an enhanced chemiluminescence reagent (Thermo Scientific). Samples were normalized to Actin (I-19) an anti-goat polyclonal antibody (Santa Cruz Biotechnology), and band density was determined using Kodak 1D imaging software.

Statistics

Data are presented as mean ± SEM from 5–6 samples for each condition for cell viability studies. Tumor masses and volumes are presented as mean ± SEM. Significance is determined by ANOVA, where $P < .05$ was considered significant.

Results

Characterization of NPs

All preparations of PLGA-NP had mean diameters of 140-160 nm, determined by scanning electron microscopy (Table 1). A representative scanning electron microscopy micrograph of NP-Bel-PGON particles showing morphology with schematic depiction is shown in Figure 1. Loading of belinostat in the PGON-functionalized NP was 3.3 and 6.8 times higher than in NP-Bel and NP-Bel-Chit, respectively (Table 1).

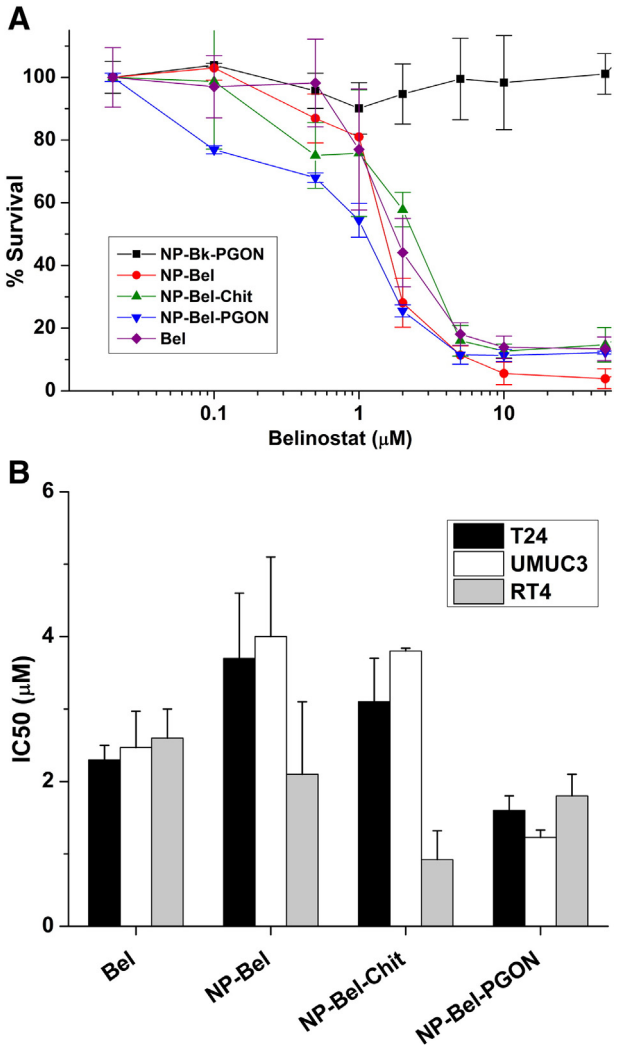

Figure 2. Effect of functionalized-belinostat loaded NPs on cell viability. (**A**) T-24 cells are incubated with increasing concentrations of Bel, NP-Bel-PGON, and NP-Bk-PGON. (**B**) IC_{50}s for Bel and NP-Bels in T-24, UM-UC-3 and RT-4 cells. Each concentration curve was done in triplicate for each cell type.

Belinostat induces urothelial cancer cytotoxicity

Viability was measured in T-24, UM-UC-3 and RT-4 bladder cancer cells, which were treated for 72 h with increasing concentrations of belinostat, provided in medium as free-drug or in NP-Bel, NP-Bel-Chit and NP-Bel-PGON formulations (Figure 2). Empty-NPs functionalized with PGON (NP-Bk-PGON, 0.0025-0.5 mg/ml) served as a negative control; these NPs did not reduce cell number, even at the highest concentrations. Viability was reduced by 70–95% in all three cell lines treated with 10 μM belinostat or functionalized belinostat NPs. Unencapsulated-belinostat has an IC_{50} of 2.5 μM whereas the IC_{50} of NP-Bel-PGON was 1.6 μM in UM-UC-3 and T-24 cells (Figure 2, *B*).

NP-Bel-PGON prolongs histone hyperacetylation in urothelial cancer cell lines

As the prime biological effect of HDACi is to induce histone acetylation, western blotting of acetylated-histone H4 from UM-UC-3R and T-24 treated cells was competed with an antibody specific for acetyl-histone H4 (Figure 3). After 30 min of treatment, acetylation was the same for the two treatment groups and only slightly above the vehicle-NP (NP-Bk-PGON).

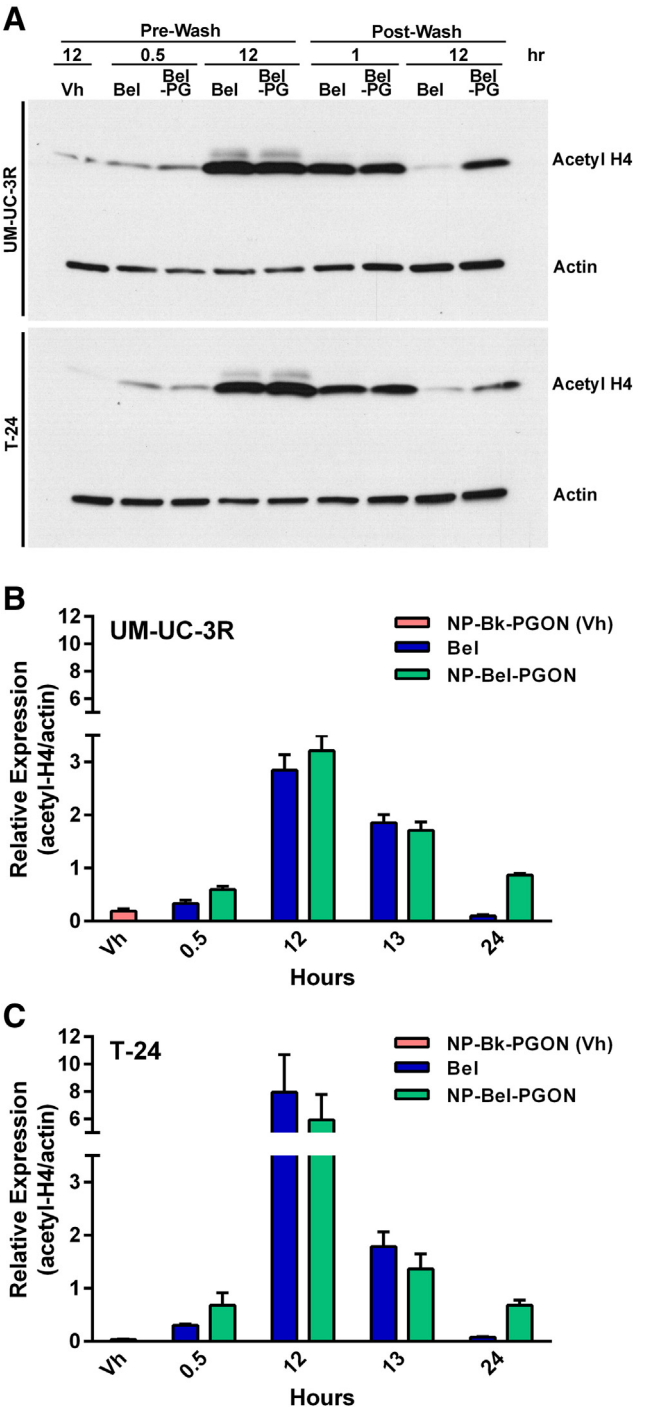

Figure 3. Acetylation activity in bladder cancer cells. (**A**) Western blot of UM-UC-3R and T-24 bladder cancer cells treated with NP-Bk-PGON, Bel, or NP-Bel-PGON. For this blot, NP-Bk-PGON is referred to as Vh, and NP-Bel-PGON as Bel-PG. Quantification of acetyl-histone H4 expression in the UM-U-C3R (**B**) and T-24 (**C**) cells from western blots in (**A**). Each concentration curve was done in at least triplicate for each cell type.

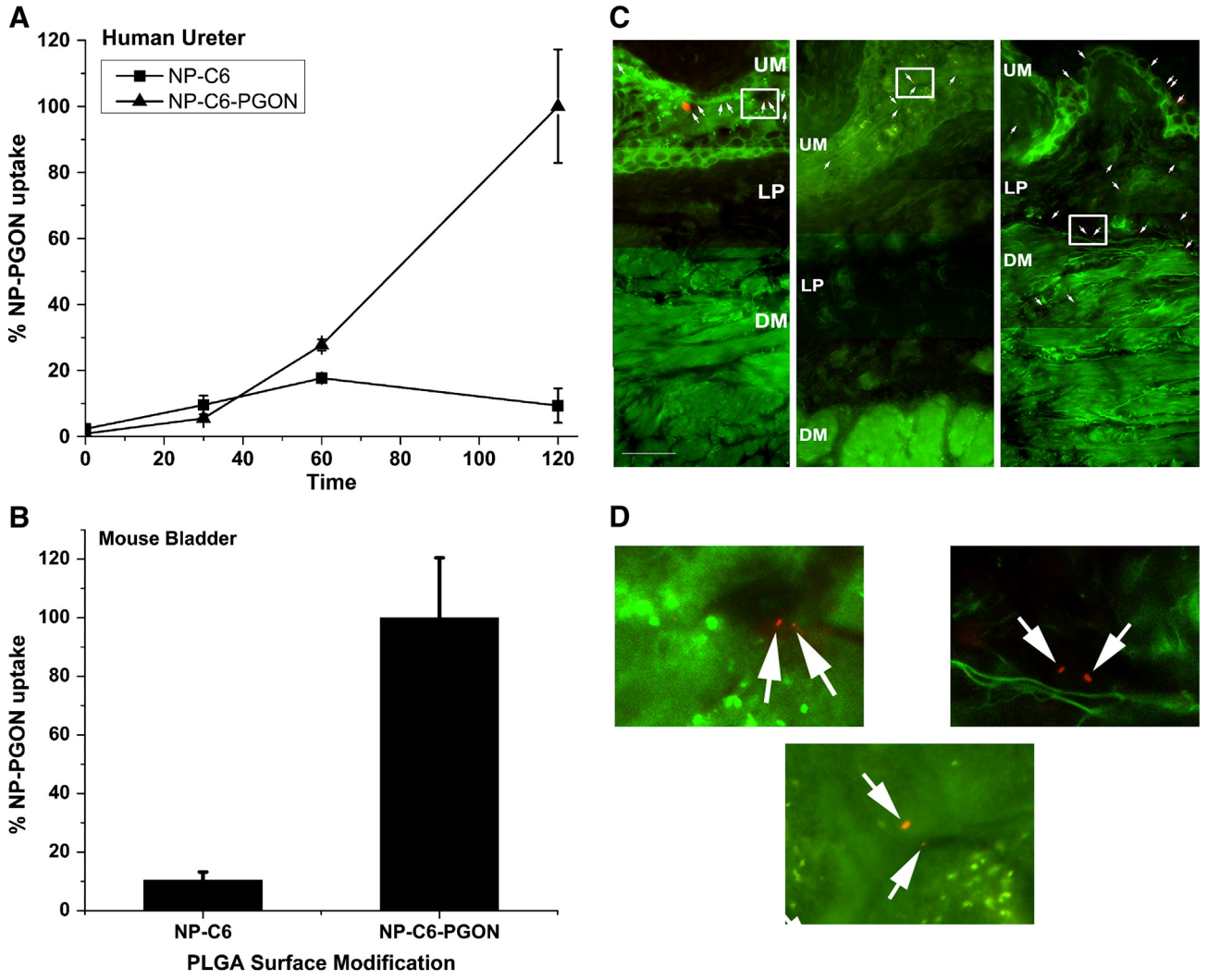

Figure 4. Uptake of functionalized coumarin-6 and nile-red NPs in human ureter and intravesically instilled mouse bladder. (**A**) Human ureter was exposed to control NPs (NP-C6) or NP-C6-PGON for 2 h and uptake of fluorescence measured. Data are expressed as % uptake of NP-C6-PGON at 120 min (n = 3 samples each from 2 ureters). (**B**) Fluorescence was measured in intravesically instilled mouse bladder after treatment for 2 h with NP-C6 control (n = 8) and NP-C6-PGON (n = 6). (**C**) Cross-sectional fluorescence microscopy images of mouse bladder intravesically instilled for 2 h with unmodified (Plain, left panel) and modified (PEG, center panel, and PGON, right panel) PLGA-NPs encapsulated with nile-red. The white arrows indicate the nile-red NPs. Multiple fields of view (at magnification, ×400) were joined to produce a continuous bladder image containing urothelium (UM), lamina propria (LP), and detrusor muscularis (DM). The scale bar represents 50 μM. (**D**) Plain (left), PEG (center), and PGON (right) represent enlarged areas of the original images (**C**) which are defined by a white square.

At 12 h of treatment, acetylated-histone H4 was over 2.5-fold higher in UM-UC-3 and over 6-fold higher in T-24 cells. When measuring relative expression to actin, encapsulated and uncapsulated belinostat were the same at 12 h of exposure in UM-UC-3R and T-24 cell lines. Histone hyperacetylation in the NP-Bel-PGON xenograft model was still evident 3 days after treatment.

One hour post-PBS wash, in drug-free medium, histone acetylation of both cell lines declined; however, acetylation was still 2-fold above baseline levels. Twelve hours post-PBS wash, the cells treated with NP-Bel-PGON continued sustained HDAC inhibition at 27% of maximum relative expression to actin in the UM-UC-3 cell line, whereas the level of histone acetylation of the unencapsulated treated cells was at baseline levels.

Penetration of BPB and internalization of NPs

NPs loaded with coumarin-6 (NP-C6), or PGON-functionalized NPs loaded with C6 (NP-C6-PGON) were incubated with human ureter over a period of 120 min. Uptake of NP-C6-PGON (200 μg NP/well) into the tissue after 2 h of incubation was 10-fold higher than that of NP-C6 (Figure 4, *A*).

Mice were intravesically instilled for 2 h with NP-C6 or NP-C6-PGON. The fluorescence from bladders treated with NP-C6-PGON was approximately 10-times that observed in bladders treated with NP-C6 (Figure 4, *B*). To identify depth of BPB penetration, microscopy of cross-sections of mouse bladders treated with NR-loaded NPs showed better urothelial and lamina propria penetration, which extended up to the surface of the detrusor muscle, with PGON-modified PLGA-NPs than with

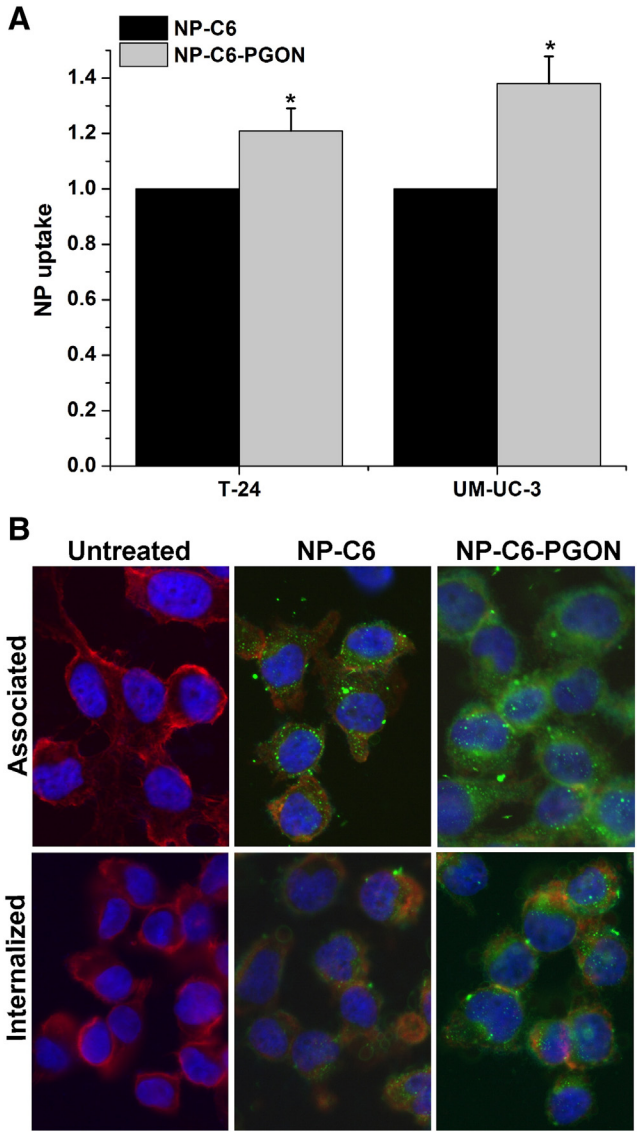

Figure 5. Internalization of PGON-modified NPs. (**A**) FACS analysis shows that NP-C6-PGON were internalized within T-24 and UM-UC-3 bladder cancer cells more efficiently than control (NP-C6). *$P < 0.05$ from control NPs (n = 3). All values were normalized to NP-C6. (**B**) Fluorescence microscopy indicated that NP-C6 and NP-C6-PGON loaded with C6 (green) were localized in the cytosol region of T-24 cells. The nucleus was stained with DAPI (blue) and the cell membrane was stained with Texas Red X-phalloidin (red).

either of the control NPs (unmodified plain-NPs or modified PEG-NPs) (Figure 4, *C*). The latter two NPs did not penetrate into the lamina propria or the detrusor muscle under these conditions.

Bladder cancer cells were incubated for 2 h with NP-C6 and NP-C6-PGON, then treated with trypan blue to quench non-internalized fluorescent NPs. FACS revealed geometric mean fluorescence values for internalized NP-C6-PGON that were greater than values from NP without surface modification by 21 ± 8% and 38 ± 10% for T-24 and UM-UC-3 cells, respectively (Figure 5, *A*). This was supported by fluorescence microscopy showing improved association and internalization when cells were treated with NP-C6-PGON (Figure 5, *B*).

Tumor response in a xenograft model

UM-UC-3R cells were injected into the flank of female Foxn1 nu/nu mice and tumors were evident in 100% of animals by 7 days. Animals were then randomized into three groups with initial tumor volumes of 236 ± 33 mm^3, 234 ± 15 mm^3 and 260 ± 21 mm^3. The tumors were subsequently treated (treatment day 0) with PBS (control), NP-Bk-PGON or NP-Bel-PGON, respectively (Figure 6). After treatment for 7 days (2 injections), tumor volumes of NP-Bel-PGON treated mice were unchanged from the pretreatment value (1.01 ± 0.1-fold) while tumor volumes of control and NP-Bk-PGON treated tumors were increased 1.56 ± 0.1 fold and 2.10 ± 0.2-fold, respectively. After 11 days (3 injections), tumor volume of NP-Bel-PGON treated mice had increased to 1.59 ± 0.3 fold of pretreatment tumor volume while tumor volume of control and NP-Bk-PGON treated tumors had increased 4.21 ± 0.7 fold and 3.58 ± 0.6 fold, respectively. At 21 days (6 injections), tumor volume of NP-Bel-PGON treated mice had stabilized at 4.59 ± 0.8 fold of pretreatment tumor volume while tumor volume of control and NP-Bk-PGON treated tumors had increased 16.46 ± 3.2 fold and 13.25 ± 2.1-fold, respectively. At 21 days, the tumor volume of NP-Bel-PGON treatment was 77% and 71% smaller than control and NP-Bk-PGON treated mice, respectively (Figure 6, *A*). A gross view of excised bladder tumors with and without a fluorescent filter is shown in Figure 6, *C*. After 21 days, the tumor weight of the NP-Bel-PGON treated mice was 62% and 52% less than the tumor weights of PBS-Con and NP-Bk-PGON treated mice, respectively (Figure 6, *B*; Table 2). For all xenograft studies, NP-Bel-PGON or nanoparticle vehicle did not cause overt toxicity or significant weight change.

The histone acetylation status of the xenograft mouse tumors (Figure 6, *D*) and those treated with NP-Bel-PGON exhibited 60% higher histone acetylation expression compared to basal levels of vehicle control. This response seen three days post treatment (on a twice weekly schedule) is similar to the *in vitro* trends.

Discussion

Currently, lesion directed resection and BCG instillation are the standard of care for non-muscle invasive bladder cancers. Unfortunately, many patients develop invasive cancer and succumb to their disease. More effective local treatment modalities at the non-muscle invasive stage could prevent morbidity and mortality. We sought to develop a nanoparticle system that could be delivered locally, adhere to and penetrate the bladder urothelium, and be internalized into urothelial cancer cells for delivery of cytotoxic agents. We have demonstrated that a NP platform to deliver belinostat using the novel amidine-based cationic polymer coating PGON for BPB penetration can confer enhanced cytotoxicity against bladder cancer cells *in vitro*, enhanced association with and transition through human and murine urothelium, extended duration of HDAC inhibition *in vitro* and *in vivo*, and reduced xenograft tumor growth.

The effect observed from NP-Bel-PGON is due to the payload, belinostat, as the vehicle did not contribute to cytotoxicity, H4 hyperacetylation or tumor response. Belinostat works through HDAC and non-histone hyperacetylation

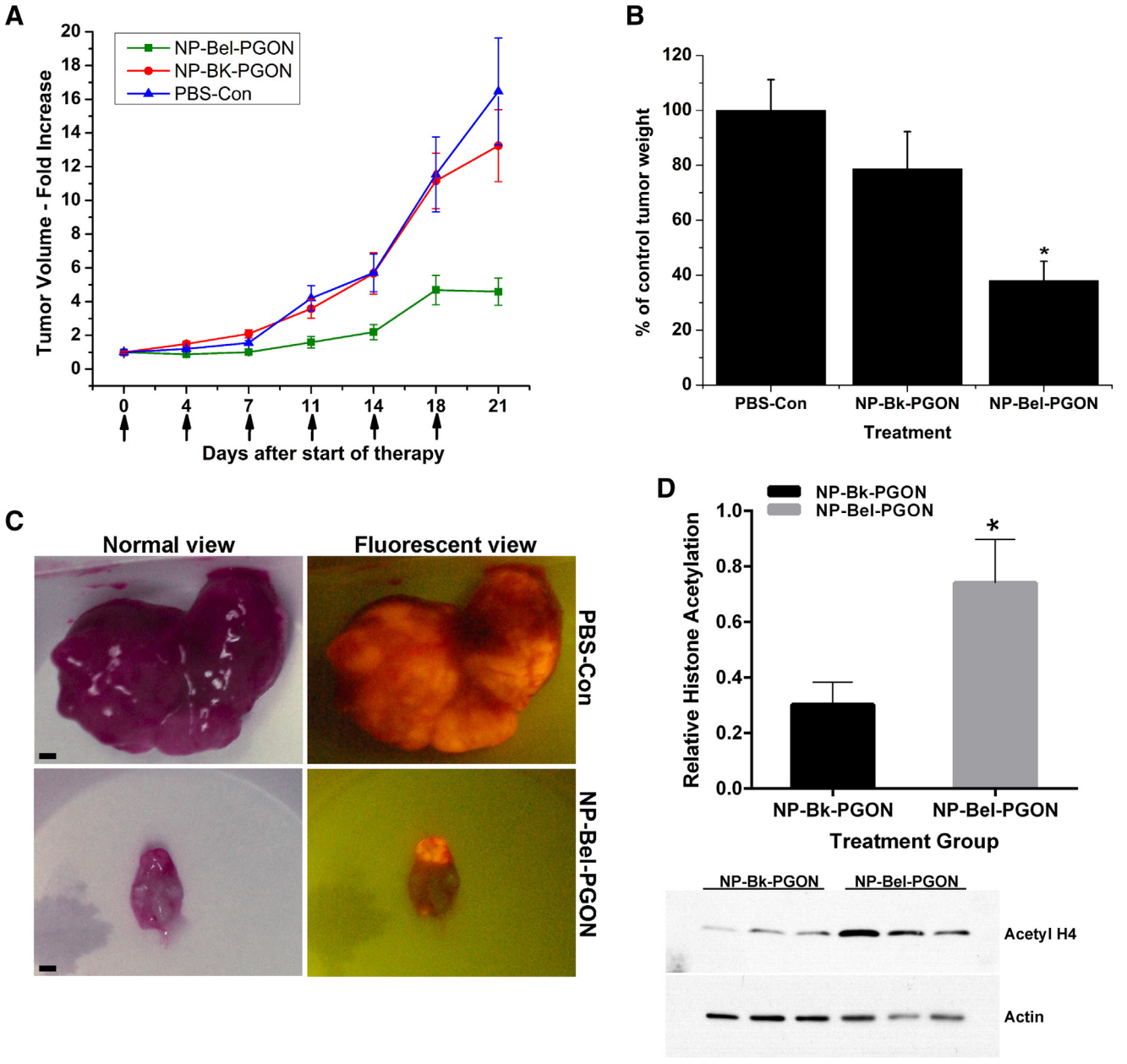

Figure 6. In vivo treatment of xenograft bladder tumors. (**A**) Seven days after flank injection of UM-UC3R cells, tumors were untreated (PBS-Con, n = 8), or injected (see arrows) a total of six times with NP-Bk-PGON (n = 12) or NP-Bel-PGON (n = 10). Tumor volumes were measured before injections and harvest day 21. All values are normalized to PBS-control. (**B**) Relative changes in tumor volume agreed well with tumor weights at 21 days. *$P < 0.05$ from control and NP-Bk-PGON. (**C**) Gross view of excised bladder tumors with and without a fluorescent filter (scale bar 1500 μM). (**D**) Western blot analysis of acetyl-histone H4 expression in excised mouse bladder tumors treated with Bk-NP-PGON (n = 6) and Bel-NP-PGON (n = 8) (bar graph). Actin expression was used to show loading equivalency and protein integrity. A representative western blot is shown.

mechanisms in the control of migration, invasion, and apoptosis in bladder cancer cell lines. Belinostat has been shown to have an IC_{50} in urothelial cancers, including bladder and prostate cancer cells,[13,14,32] in the 1–10 μM range and is corroborated by our findings of 2–3 μM. Belinostat is currently used in clinical trials where intravenous treatment consists of daily infusions that reach approximately 100 μM at C_{max} with short-lived (<6 h) histone acetylation states in peripheral blood mononuclear cells,[18] which have been shown in animal models to surrogate for tumor tissue acetylation state.[33]

Few studies have used nanoencapsulated HDAC inhibitors for treatment of cancer. One involved encapsulation of belinostat into a liposome using a lipid film hydration technique.[34] Belinostat encapsulated in the liposome exhibited similar IC_{50} to unencapsulated belinostat, hyperacetylation of histone H4 in MCF-7 breast cancer cells, and biologic activity during 24 hours of continuous *in vitro* exposure.[34] Our data using a ligand enhanced polymeric NP system similarly achieves a small size that increases the likelihood of transiting through disruptions in the BPB. Though the optimal size for this setting has not been

Table 2
Final tumor mass after 3 weeks of treatment.

Treatment	n	Tumor mass ± SEM (mg)
NP-Bk-PGON	12	2145 ± 369
PBS-Con	8	2725 ± 306
NP-Bel-PGON	10	1037 ± 190[§,‖]

n = number of animals in each group. [§]$P < 0.05$ from PBS treated tumors and [‖]$P < 0.05$ from NP-Bk-PGON treated tumors.

evaluated, and it is unclear if there may even be diminishing returns with diminishing size, our data support the benefit of using a PGON penetrating polymer surface modification. In addition, we have shown that NP-Bel-PGONs cause histone H4 hyperacetylation in two urothelial cancer cell lines within 30 min of exposure, which suggests an initial burst release profile that was maintained for 3 days. Another study involved encapsulation of sulforaphane into albumin microspheres, and resulted in a reduction in tumor growth.[35]

We synthesized PLGA-NPs because they are biocompatible and biodegradable polymers that can be functionalized with polymers and peptides.[25,26] PGON is a cationic polymer with positively charged guanidinium groups[27] that can overcome PLGA repulsion from the anionic glycosaminoglycan coated apical surface of urothelial cells and lead to enhanced penetration and uptake. PGON was proposed for local bladder delivery as it penetrates eukaryotic cells without apparent toxicity and may facilitate cellular entry of the nanoparticle payload. The polycationic PGON could help the NPs adhere to the bladder wall and even open cellular junctions similar to other positively charged polymers.[36–38] Here, we examined uptake of NP-PGON loaded with the C6 fluorophore in human ureter. Uptake of PGON-functionalized nanoparticles was linear for 2 h. Using fluorescently labeled PGON-functionalized NPs, we achieved a 10-fold increase in uptake in *ex vivo* human ureter and in *in vivo* mouse bladder compared to control NPs and greater penetration through the urothelium compared to control PEG-modified NPs. PGON-functionalized NPs penetrated into the lamina propria up to the surface of the detrusor muscle in mouse bladder.

Because of its penetration capabilities, PGON-functionalized NPs were loaded with belinostat for testing against xenograft tumors. Belinostat loaded more efficiently into PGON NPs compared to the unmodified or palmitoylated avidin chitosan-coated NPs. This may be due to a more favorable hydrophobic-hydrophilic interaction of belinostat with the PEGylated-lipid (DSPE-PEG) that confers a loading efficiency advantage over unmodified NPs or palmitoylated-avidin. Chitosan could not be made to surface coat PLGA-NP with the DSPE-PEG anchor system. Nonetheless, equimolar belinostat concentrations were used for all comparisons and showed similar cytotoxicity *in vitro* (Figure 2, *A*) as well as similar pre-wash histone H4 hyperacetylation. Vehicle controls of PGON coated PLGA-NPs were cell and tumor growth-neutral and did not alter histone acetylation expression.

To test our delivery system in an *in vivo* bladder cancer model, we used the UM-UC-3R human bladder cancer cell line in a flank xenograft murine model as it is a well characterized model that allowed for local therapy in a controlled manner. The *in vitro* washout and internalization studies showed the UM-UC-3R cells internalize the belinostat NPs and preserve a histone hyperacetylation state for a longer duration than unencapsulated drug.[39–41] Using NPs, we provided an *in vivo* dose of belinostat that was ~100 times the IC_{50} for bladder cancer cells. When functionalized with PGON, belinostat-loaded NPs that were injected into the tumors reduced tumor growth for at least 11 days, while tumor volume of control and NP-Bk-PGON injected tumors doubled. After 3 weeks, the tumor weight in animals treated with NP-Bel-PGON was less than half of that of vehicle control. In addition to the size difference, postmortem tumor RFP fluorescence suggests that the NP-Bel-PGON treated tumors comprised a smaller proportion of live neoplastic cells than the untreated or NP-Bk-PGON treated tumors. The larger non-fluorescent area in the NP-Bel-PGON treated group may represent apoptotic or necrotic areas, or attenuated RFP expression in the ongoing presence of HDAC inhibition perhaps due to epigenetic modification such as alternative splicing[42] or hyperacetylation of non-histone proteins that are requisite for fluorescence.

While our *in vitro* data are similar to other studies of bladder and prostate cancer cells treated with belinostat, notable differences are prominent in our *in vivo* studies. Previous pharmacokinetic and tumor pharmacodynamic studies in similar Foxn1 nude urothelial cancer have shown that non-encapsulated belinostat peaks in tumor tissue as well as in plasma and spleen at 1 h with a return to baseline after 3 h, and does not distribute in a tumor specific manner.[33] Therefore, frequent dosing of belinostat has been shown to reduce tumor growth of human cancer xenografts in nude mice with dosing of 40 mg/kg once to thrice daily for up to three weeks.[12,13,43] These frequent dosing approaches have served as the basis for all xenograft studies of belinostat. As our system is designed for local bladder delivery and based on the prolonged duration of histone hyperacetylation from *in vitro* studies, we chose a twice weekly local delivery approach at a dose of 5 mg/kg belinostat extrapolated from *in vitro* cytotoxicity and washout data. Incidentally, at the start of treatment, the weights of all mice were within 2 mg of each other, resulting in the same dose, thereby avoiding systematic error of dosing locally based on a whole mouse mass.

Pharmacokinetic and pharmacodynamic studies of systemic delivery via intravenous belinostat in humans given over 30 min has demonstrated a half-life under 90 min, with H4 hyperacetylation of circulating peripheral blood mononuclear cells at 4 times control for approximately 2–6 h.[18] Our *in vitro* study showed that the UM-UC-3R cells still had 4.5 times more hyperacetylation of histone H4 than vehicle control 12 h after wash (Figure 3, *B*) and tumor histone hyperacetylation in the NP-Bel-PGON xenograft group was still evident three days after treatment. Importantly, the NP vehicle was tumor growth neutral and 6 injections of NP-PGON containing 5 mg/kg belinostat over 21 days reduced tumor volume 71% compared to vehicle. In a transgenic model in which H-RAS was constitutively expressed under the control of a bladder urothelium mouse uroplakin II promoter, belinostat was given intraperitoneally at a dose of 100 mg/kg for 5 days a week for three weeks. The bladder weight for belinostat treated mice versus controls was reduced 50% in males and 36% in females.[14] In an orthotopic prostate cancer tumor model, belinostat was administered intraperitoneally at a dose of

40 mg/kg, three times a day for 3 weeks[13] and led to tumor growth reduction of 43% relative to the vehicle treated group.

Our data show that the PGON-NPs adhere to and penetrate the urothelium, are taken up by bladder cancer cells, have neutral tumor growth effect, and when encapsulated with belinostat, can cause sustained HDAC inhibition and tumor kill. Thus, our study suggests that an improved therapeutic index may be achieved with local delivery of a polymeric NP surface-modified with the novel polymer, PGON.

Acknowledgments

We thank Rachel Fields, PhD for preparation of palmitoylated avidin. Belinostat was provided by the National Cancer Institute Cancer Therapy Evaluation Program as an agent proprietary to TopoTarget.

References

1. Baffa R, Letko J, McClung C, LeNoir J, Vecchione A, Gomella LG. Molecular genetics of bladder cancer: targets for diagnosis and therapy. *J Exp Clin Cancer Res: CR* 2006;**25**:145-60.
2. Alexandroff AB, Jackson AM, O'Donnell MA, James K. BCG immunotherapy of bladder cancer: 20 years on. *Lancet* 1999;**353**: 1689-94.
3. GuhaSarkar S, Banerjee R. Intravesical drug delivery: Challenges, current status, opportunities and novel strategies. *J Control Release* 2010;**148**:147-59.
4. Gurpinar T, Truong LD, Wong HY, Griffith DP. Electromotive drug administration to the urinary bladder: an animal model and preliminary results. *J Urol* 1996;**156**:1496-501.
5. Di Stasi SM, Valenti M, Verri C, et al. Electromotive instillation of mitomycin immediately before transurethral resection for patients with primary urothelial non-muscle invasive bladder cancer: a randomised controlled trial. *Lancet Oncol* 2011;**12**:871-9.
6. Di Stasi SM, Giannantoni A, Stephen RL, et al. Intravesical electromotive mitomycin C versus passive transport mitomycin C for high risk superficial bladder cancer: a prospective randomized study. *J Urol* 2003;**170**:777-82.
7. Barocas DA, Globe DR, Colayco D, et al. Surveillance and treatment of non-muscle-invasive bladder cancer in the USA. *Adv Urol* 2012;**2012**:8.
8. Chiba T, Yokosuka O, Arai M, et al. Identification of genes up-regulated by histone deacetylase inhibition with cDNA microarray and exploration of epigenetic alterations on hepatoma cells. *J Hepatol* 2004;**41**:436-45.
9. Glaser KB, Staver MJ, Waring JF, Stender J, Ulrich RG, Davidsen SK. Gene expression profiling of multiple histone deacetylase (HDAC) inhibitors: defining a common gene set produced by HDAC inhibition in T24 and MDA carcinoma cell lines. *Mol Cancer Ther* 2003;**2**:151-63.
10. Lee H, Lee S, Baek M, Kim H-Y, Jeoung D-I. Expression profile analysis of trichostatin A in human gastric cancer cells. *Biotechnol Lett* 2002;**24**:377-81.
11. Marks PA, Richon VM, Rifkind RA. Histone deacetylase inhibitors: inducers of differentiation or apoptosis of transformed cells. *J Natl Cancer Inst* 2000;**92**:1210-6.
12. Tran AD-A, Marmo TP, Salam AA, et al. HDAC6 deacetylation of tubulin modulates dynamics of cellular adhesions. *J Cell Sci* 2007;**120**: 1469-79.
13. Qian X, Ara G, Mills E, LaRochelle WJ, Lichenstein HS, Jeffers M. Activity of the histone deacetylase inhibitor belinostat (PXD101) in preclinical models of prostate cancer. *Int J Cancer J Int du Cancer* 2008;**122**:1400-10.
14. Buckley MT, Yoon J, Yee H, et al. The histone deacetylase inhibitor belinostat (PXD101) suppresses bladder cancer cell growth in vitro and in vivo. *J Transl Med* 2007;**5**:49.
15. Gould JJ, Kenney PA, Rieger-Christ KM, et al. Identification of tumor and invasion suppressor gene modulators in bladder cancer by different classes of histone deacetylase inhibitors using reverse phase protein arrays. *J Urol* 2010;**183**:2395-402.
16. Chowdhury S, Howell GM, Teggart CA, et al. Histone deacetylase inhibitor belinostat represses survivin expression through reactivation of transforming growth factor β (TGFβ) receptor II leading to cancer cell death. *J Biol Chem* 2011;**286**:30937-48.
17. Portland VA Medical Center. Chemoprevention of Prostate Cancer, HDAC Inhibition and DNA Methylation. Bethesda (MD): National Library of Medicine (US). 2013; NLM Identifier: NCT01265953.
18. Steele NL, Plumb JA, Vidal L, et al. A phase 1 pharmacokinetic and pharmacodynamic study of the histone deacetylase inhibitor belinostat in patients with advanced solid tumors. *Clin Cancer Res* 2008;**14**:804-10.
19. Khan A, Benboubetra M, Sayyed PZ, et al. Sustained polymeric delivery of gene silencing antisense ODNs, siRNA, DNAzymes and ribozymes: in vitro and in vivo studies. *J Drug Target* 2004;**12**:393-404.
20. Anthony T, Fong P, Goyal A, Saltzman WM, Moss RL, Breuer C. Development of a parathyroid hormone-controlled release system as a potential surgical treatment for hypoparathyroidism. *J Pediatr Surg* 2005;**40**:81-5.
21. Woodrow KA, Cu Y, Booth CJ, Saucier-Sawyer JK, Wood MJ, Saltzman WM. Intravaginal gene silencing using biodegradable polymer nanoparticles densely loaded with small-interfering RNA. *Nat Mater* 2009;**8**:526-33.
22. Cu Y, Booth CJ, Saltzman WM. In vivo distribution of surface-modified PLGA nanoparticles following intravaginal delivery. *J Control Release* 2011;**156**:258-64.
23. Zhou J, Patel TR, Fu M, Bertram JP, Saltzman WM. Octa-functional PLGA nanoparticles for targeted and efficient siRNA delivery to tumors. *Biomaterials* 2012;**33**:583-91.
24. Sawyer AJ, Saucier-Sawyer JK, Booth CJ, et al. Convection-enhanced delivery of camptothecin-loaded polymer nanoparticles for treatment of intracranial tumors. *Drug Delivery Transl Res* 2011;**1**:34-42.
25. Cheng CJ, Saltzman WM. Enhanced siRNA delivery into cells by exploiting the synergy between targeting ligands and cell-penetrating peptides. *Biomaterials* 2011;**32**:6194-203.
26. Fahmy TM, Samstein RM, Harness CC, Mark Saltzman W. Surface modification of biodegradable polyesters with fatty acid conjugates for improved drug targeting. *Biomaterials* 2005;**26**:5727-36.
27. Hennig A, Gabriel GJ, Tew GN, Matile S. Stimuli-responsive polyguanidino-oxanorbornene membrane transporters as multicomponent sensors in complex matrices. *J Am Chem Soc* 2008;**130**: 10338-44.
28. Gabriel GJ, Madkour AE, Dabkowski JM, Nelson CF, Nusslein K, Tew GN. Synthetic mimic of antimicrobial peptide with nonmembrane-disrupting antibacterial properties. *Biomacromolecules* 2008;**9**: 2980-3.
29. Martin DT, Steinbach J, Kaimakliotis H, et al. Surface modifications of poly(lactide-co-glycolide) nanoparticles can increase its uptake by bladder cancer cells. *J Urol* 2011;**185**:e424.
30. Takizawa BT, Uchio EM, Cohen JJ, Wheeler MA, Weiss RM. Downregulation of survivin is associated with reductions in TNF receptors' mRNA and protein and alterations in nuclear factor kappa B signaling in urothelial cancer cells. *Cancer Invest* 2007;**25**:678-84.
31. Martin DT, Gendron RL, Jarzembowski JA, et al. Tubedown expression correlates with the differentiation status and aggressiveness of neuroblastic tumors. *Clin Cancer Res* 2007;**13**:1480-7.
32. Kuefer R, Hofer MD, Altug V, et al. Sodium butyrate and tributyrin induce in vivo growth inhibition and apoptosis in human prostate cancer. *Br J Cancer* 2004;**90**:535-41.
33. Marquard L, Petersen KD, Persson M, Hoff KD, Jensen PB, Sehested M. Monitoring the effect of belinostat in solid tumors by H4 acetylation. *APMIS: Acta pathologica, microbiologica, et immunologica scand* 2008;**116**:382-92.

34. Urbinati G, Marsaud V, Plassat V, Fattal E, Lesieur S, Renoir JM. Liposomes loaded with histone deacetylase inhibitors for breast cancer therapy. *Int J Pharm* 2010;**397**:184-93.
35. Do DP, Pai SB, Rizvi SA, D'Souza MJ. Development of sulforaphane-encapsulated microspheres for cancer epigenetic therapy. *Int J Pharm* 2010;**386**:114-21.
36. Seiler MW, Venkatachalam MA, Cotran RS. Glomerular epithelium: structural alterations induced by polycations. *Science* 1975;**189**:390-3.
37. Quinton PM, Philpott CW. A role for anionic sites in epithelial architecture. Effects of cationic polymers on cell membrane structure. *J Cell Biol* 1973;**56**:787-96.
38. Lavelle J, Meyers S, Ramage R, et al. Bladder permeability barrier: recovery from selective injury of surface epithelial cells. *Am J Physiol Renal Physiol* 2002;**283**:F242-53.
39. Muramaki M, Miyake H, Hara I, Kamidono S. Introduction of midkine gene into human bladder cancer cells enhances their malignant phenotype but increases their sensitivity to antiangiogenic therapy. *Clin Cancer Res* 2003;**9**:5152-60.
40. Tanaka M, Grossman HB. Connexin 26 gene therapy of human bladder cancer: induction of growth suppression, apoptosis, and synergy with Cisplatin. *Hum Gene Ther* 2001;**12**:2225-36.
41. Nakahara T, Kita A, Yamanaka K, et al. Broad spectrum and potent antitumor activities of YM155, a novel small-molecule survivin suppressant, in a wide variety of human cancer cell lines and xenograft models. *Cancer Sci* 2011;**102**:614-21.
42. Hnilicová J, Hozeifi S, Dušková E, Icha J, Tománková T, Staněk D. Histone deacetylase activity modulates alternative splicing. *PLoS One* 2011;**6**:e16727.
43. Plumb JA, Finn PW, Williams RJ, et al. Pharmacodynamic response and inhibition of growth of human tumor xenografts by the novel histone deacetylase inhibitor PXD101. *Mol Cancer Ther* 2003;**2**: 721-8.